Journal of Power Sources 208 (2012) 257–262

Contents lists available at SciVerse ScienceDirect

Journal of Power Sources

journal homepage: www.elsevier.com/locate/jpowsour

Fundamental studies on direct ammonia fuel cell employing anion exchange membrane

Shohei Suzuki, Hiroki Muroyama, Toshiaki Matsui, Koichi Eguchi *

Department of Energy and Hydrocarbon Chemistry, Graduate School of Engineering, Kyoto University, Nishikyo-ku, Kyoto 615-8510, Japan

ARTICLE INFO

Article history:
Received 20 November 2011
Received in revised form 31 January 2012
Accepted 14 February 2012
Available online 22 February 2012

Keywords:
Anion exchange membrane
Direct ammonia fuel cell
Electrocatalyst
Ammonia oxidation
Atomic nitrogen adspecies

ABSTRACT

The fundamental characteristics of direct ammonia fuel cell employing anion exchange membrane (AEM) as an electrolyte was evaluated. The fuel cells with three different anodes of Pt/C, Pt–Ru/C, and Ru/C were applied for the performance tests. The open circuit voltage (OCV) was notably lower than the ideal electromotive force of 1.17 V and significantly dependent on the electrocatalysts. The OCV achieved was in the following sequence: Pt–Ru/C > Pt/C > Ru/C. Furthermore, the ammonia permeated through the AEM by the solubility–diffusion mechanism and the formation of oxidants such as N_2 and NO was detected in the cathode exhaust gas. This result indicates the oxidation of ammonia in the cathode, which will be another factor for the reduction in OCV. Note that OCV and performance continuously decreased during the consecutive *I–V* characteristic measurements because of the N_{ad} poisoning over the surface of anode catalysts.

1. Introduction

Hydrogen is the main fuel source for power generation with fuel cells, but its low volumetric energy density is the main obstacle for the application in transportable devices and automobiles. To overcome this problem, hydrogen careers such as methanol and $NaBH_4$ have been proposed as alternative fuels for fuel cell systems [1,2]. Among them, ammonia is one of the promising candidates due to its low production cost, ease in liquefaction at ambient temperatures, and high energy density [3–5]. However, the ammonia only serves as the degradation factor in polymer electrolyte fuel cells (PEFCs) employing an acidic electrolytes such as Nafion® [6–8]. Even a trace amount of ammonia (1–10 ppm) in a hydrogen fuel causes serious performance deterioration. This is because the replacement of H^+ by NH_4^+ ions both in the catalyst layer ionomer and in bulk membrane leads to the reduction in conductivity. In contrast, ammonia can be electrochemically oxidized in an alkaline electrolyte, and the conventional alkaline fuel cell using potassium hydroxide (KOH) as an electrolyte was operated successfully with directly supplying ammonia [9–11].

In these circumstances, anion exchange membranes (AEMs) have been attracted much attention for PEFC electrolytes [12]. The AEMs are alkaline polymers containing quaternary ammonium or pyridinium functional groups as ion exchange sites. Although the performance of conventional alkaline fuel cell degrades seriously by the formation of carbonate salts in the cathode via the chemical reaction between KOH and CO_2 [13,14], in AEMs such carbonate salts are not formed due to the absence of free cation like K^+ [15]. Thus, AEMs are considered as promising electrolytes for the direct ammonia fuel cells. Recently, the power generation of the direct ammonia fuel cell using an anion exchange membrane was demonstrated by Lan and Tao [16]. However, they only showed the performance with a maximum power density of 0.7 mW cm^{-2} and 16 mW cm^{-2} with Pt–Ru/C anode and Cr-decorated Ni/C anode, respectively, and the reason for the performance limitation has not been discussed. For the further enhancement of performance, the development and optimization of electrocatalyst as well as AEM are required.

Many studies on the electrochemical ammonia oxidation over Pt electrode in an alkaline aqueous electrolyte have been reported. Gerischer and Mauerer proposed the ammonia oxidation mechanism including the production of poisoning species [17], which has been supported by the coulometric experiments [18], differential electrochemical mass spectroscopy (DEMS) [19,20], and surface enhanced Raman spectroscopy (SERS) [21,22]. According to this mechanism, NH_{2ad} and NH_{ad} adsorbed species are produced over Pt electrode by the sequential ammonia dehydrogenation, and subsequently combined to form N_2H_{xad} (x = 2–4). Finally, further dehydrogenation of N_2H_{xad} leads to the formation of N_2. On the other hand, the fully dehydrogenated adsorbate, atomic nitrogen adspecies (N_{ad}), is inert for N_2 formation and acts as a poisoning species on electrodes. de Vooys et al. [20] studied the ammonia oxidation over the platinum group metals (Pt, Ru, Pd, Rh, and Ir), and found that N_{ad} served as a poisoning species on those

* Corresponding author. Tel.: +81 75 383 2519; fax: +81 75 383 2520.
E-mail address: eguchi@scl.kyoto-u.ac.jp (K. Eguchi).

0378-7753/$ – see front matter © 2012 Elsevier B.V. All rights reserved.
doi:10.1016/j.jpowsour.2012.02.043

Table 1
Basic properties of AEM (A201, Tokuyama Co.)..

Property	
Thickness (μm)	28
Ion-exchange capacity (mmol g^{-1})	1.7
Water content[a] (wt%)	25
OH^- conductivity (mS cm^{-1})	42

[a] Gravimetric water content of the fully hydrated membranes.

metals. The electrocatalytic activity for the ammonia oxidation varied in the order of Ru < Rh < Pd < Ir < Pt. This order in catalytic activity reflected the difference in the affinity of N_{ad} for the metal surface. The activity enhancement of Pt-based catalysts was achieved by using the Pt–M binary alloys (M = Ir, Ru) [23,24]. As described above, the ammonia oxidation in an alkaline aqueous solution was significantly affected by the formation of N_{ad} and the electrode materials. For direct ammonia fuel cells, however, the influence of these factors on the performance has not been yet discussed in detail.

In this study, then, the fundamental characteristics of the direct ammonia fuel cell with an anion exchange membrane were evaluated; especially, the influence of anode materials on the cell performance was analyzed.

2. Experimental

2.1. Catalyst preparation

The electrocatalysts of Pt/C, Pt–Ru/C, and Ru/C were used for electrochemical measurements. Pt/C (Pt: 46.4 wt%, Tanaka Kikinzoku Kogyo) and Pt–Ru/C (Pt: 30 wt%, Ru: 15 wt%, Johonson–Matthey) were commercially available regents, and the Ru/C catalyst was prepared by the impregnation method. A mixture of $Ru(NO_3)_3$ solution (Tanaka Kikinzoku Kogyo) and carbon black (Vulcan XC-72, Cabot Co.) was kept on a steam bath at 80 °C until the solvent was evaporated. The Ru loading was fixed at 20 wt%. The resulting powder was pretreated in 20% H_2–N_2 at 400 °C for 30 min.

2.2. Cyclic voltammetry

Cyclic voltammograms of the catalysts in 1 M KOH or 0.1 M NH_3–1 M KOH solution were recorded by the following procedure. A suspension containing the catalyst in water was ultrasonically dispersed for 30 min, and then dropped onto the glassy carbon disk electrode (0.196 cm^2). The loading amount of noble metal on the electrode was 28 μg cm^{-2}. After the water evaporated, the electrode surface was covered with 10 μl of anion exchange ionomer solution (AS-4, Tokuyama Corp., diluted to 1 wt% solution with ethanol). The platinum wire and reversible hydrogen electrode (RHE) were used as counter and reference electrodes, respectively, in the conventional three-electrode cell. The electrolyte solutions were prepared with 28 wt% NH_3 solution (Wako Pure Chemical), KOH (Sigma–Aldrich, >85 wt%), and ultrapure water (Milipore MiliQ). After deoxygenation in the electrolyte solution by purging Ar, cyclic voltammetry was conducted at 25 °C using HSV-100 (Hokuto Denko) with a scanning rate of 20 mV s^{-1}.

2.3. Fuel cell test

The basic properties of the anion exchange membrane (A201, Tokuyama Corp.) used in this study are summarized in Table 1. The catalyst inks were prepared by ultrasonically mixing anion exchange ionomer solution and the electrocatalysts for 30 min. Then, the resultant ink was stirred overnight. Membrane electrode assembly (MEA) was obtained by screen-printing this ink on the anion exchange membrane. The Pt/C electrocatalyst was applied for the cathode in all cases while the anode was composed of either Pt/C, Pt–Ru/C, or Ru/C catalysts. The electrode area was 5.0 cm^2 and the ionomer content was 0.5 mg cm^{-2} in the electrodes. The loading amount of noble metal was 0.5 mg cm^{-2} in Pt/C and Pt–Ru/C, and 1.2 mg cm^{-2} in Ru/C. This MEA was immersed in 1 M KOH solution for over 6 h to obtain OH^--form AEM by ion-exchange. After that, in an Ar atmosphere, the MEA was rinsed several times with distilled water and set in the fuel cell housing as shown in Fig. 1. The experiments were carried out at 50 °C. Hydrogen and/or ammonia were fed to the anode, and 21% O_2–N_2 to the cathode. The flow rates of feeding gases were 100 ml min^{-1} for H_2 and 21% O_2–N_2, and 15 ml min^{-1} for NH_3. The feeding gases of H_2 and O_2–N_2 mixture were bubbled through water. The humidified ammonia gas was prepared by bubbling through the saturated ammonia aqueous solution. The bubbling temperature was controlled to be the same as the fuel cell operating one. Electrochemical measurements were conducted with Solartron 1287 potentiostat and Solartron 1260 frequency response analyzer. *I–V* characteristics were measured with scanning rate of 1 mV s^{-1}.

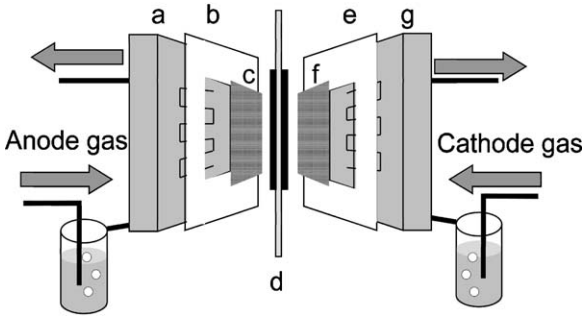

Fig. 1. Schematic diagram of the anion exchange membrane fuel cell configuration: (a and g) graphite blocks with serpentine flow field; (b and e) Teflon gasket; (c and f) carbon paper backings; (d) membrane electrode assembly.

In some cases, the exhaust gas at the cathode was analyzed by the quadrupol mass spectrometer (Canon ANELVA Corp.); the fuel cell was operated at 20 °C with a supply of 21% O_2–Ar to the cathode to detect N_2 and NO formed.

2.4. Gas permeability

The ammonia permeability of AEM was examined under wet and dry conditions at 50 °C. The AEM was set in the same housing as in the case of fuel cell operation. In a dry condition a gaseous mixture of NH_3–Ar was supplied to one side, and nitrogen was fed to the other side. In a wet condition, the feeding gases in both sides were fully humidified by the same way as described in Section 2.3. The permeated NH_3 gas was trapped by passing the exhaust gas in nitrogen side through pure water. The ammonia molar quantity in the obtained solution was determined by the acid–base titration with 0.1 M HCl and the phenolphthalein indicator.

The hydrogen permeability through the membrane was measured at 50 °C with a GTR-200XFTS (GTR Tech Corp.) gas permeation measurement apparatus equipped with a gas chromatograph (G2700, Yanaco Analytical Systams, Inc.). A membrane sample was set in a cell. On one side of the membrane, hydrogen gas was supplied at a flow rate of 30 ml min^{-1}, while on the other side argon gas was supplied at a flow rate of 30 ml min^{-1}. The feeding gases in both sides were humidified to the relative humidity of 90% before supplying to the cell. The exhaust gas from argon side was analyzed by gas chromatograph to detect the hydrogen. The molar quantity of the permeated hydrogen was calculated with the ideal gas approximation.

The gas flux permeated through the AEM, J, was calculated from the following equation:

$$J = \frac{n}{At} \quad (1)$$

where n is the obtained molar quantity of permeated gas, t is the sampling time, and A is the contact area with the supplied gas. If the gas permeation across the AEM obeys the solubility–diffusion mechanism, the permeated gas flux of J will vary linearly with the difference in the partial pressure of both sides (p) [25]. The permeability coefficient, P, was evaluated by the following equation:

$$P = \frac{Jl}{p} \quad (2)$$

where l is the membrane thickness. In this study, p was defined as the partial pressure of target gas at the supply side because the partial pressure was much larger than that at the other side.

3. Results and discussion

3.1. Ammonia oxidation in alkaline aqueous solutions

The electrochemical ammonia oxidation reaction over electrocatalysts was studied by the cyclic voltammetry in alkaline aqueous solutions. Fig. 2 shows the cyclic voltammograms of (a) Pt/C, (b) Pt–Ru/C, and (c) Ru/C electrocatalysts under the presence and absence of 0.1 M ammonia in 1 M KOH in the sweep range of 0.05–0.90 V. The onset potentials of ammonia oxidation were ca. 0.45 V and 0.30 V for Pt/C and Pt–Ru/C, respectively. This result agreed well with the previous reports [23,24]. The peak current of ammonia oxidation was obtained at ca. 0.65 V and 0.70 V in Pt/C and Pt–Ru/C, respectively, and the maximum current achieved was in the order of Pt/C > Pt–Ru/C. It was reported that the ammonia oxidation current was larger for Pt–Ru with a molar ratio of 4:1 than for Pt and significantly decreased with increasing Ru content in Pt–Ru [23,24]. The difference in the maximum current is attributable to the Ru content in the electrocatalysts. For Ru/C, the ammonia oxidation was initiated at ca. 0.30 V with a small oxidation current. This behavior is originated from the low catalytic activity of Ru metal for the production of N_2; no continuous oxidation current of ammonia was observed over Ru/C during potentiostatic polarization in the range of 0.05–0.80 V (vs. RHE) [20]. For each catalyst, the voltammograms remained unchanged even further consecutive measurements in this potential range of 0.05–0.90 V.

Fig. 3 shows the cyclic voltammograms of Pt/C in the sweep range of 0.50–0.90 V in 1 M KOH solution with 0.1 M ammonia during the tenth-consecutive measurements. Note that the current density of ammonia oxidation decreased with an increase in scanning times. This peculiar behavior was attributed to the accumulation of N_{ad} on Pt surface above 0.56 V (vs. RHE) [18]. The reductive stripping of the accumulated adsorbed species on Pt surface occurs in the hydrogen adsorption region [18], which could be confirmed as the reduction current at around 0.40 V shown in Fig. 2. Similar phenomenon was confirmed for Pt–Ru/C (not shown), attributable to the same mechanism of the N_{ad} poisoning [23,26].

3.2. H_2–O_2 fuel cells

The current–voltage characteristics of single cells employing three different anodes with a supply of hydrogen fuel are displayed in Fig. 4. Three cells exhibited almost the same open circuit voltage (OCV) regardless of anode materials. This value was lower than the theoretical value of 1.23 V, but comparable to the reported ones for the cell with Pt/C electrode [27]. The obtained cell performance varied in the order of Pt/C ≈ Pt–Ru/C > Ru/C; the performance of the cell with Pt/C was relatively high as compared to the reported AEM fuel

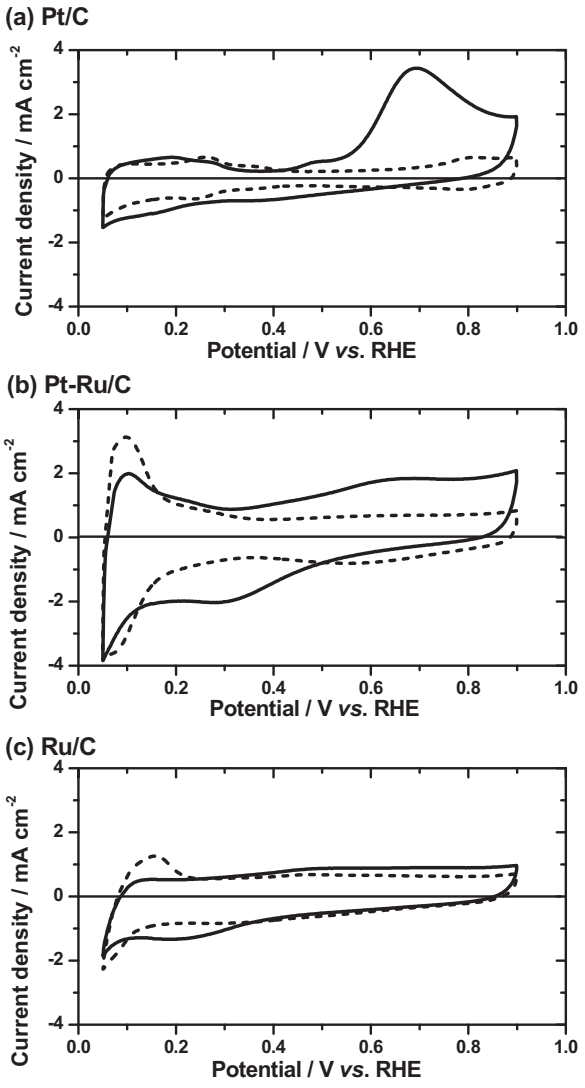

Fig. 2. Cyclic voltammograms of (a) Pt/C, (b) Pt–Ru/C, and (c) Ru/C in the presence (solid line) and absence (broken line) of 0.1 M NH_3 in 1 M KOH at 25 °C. Sweep range: 0.05–0.90 V; scanning rate: 20 mV s^{-1}.

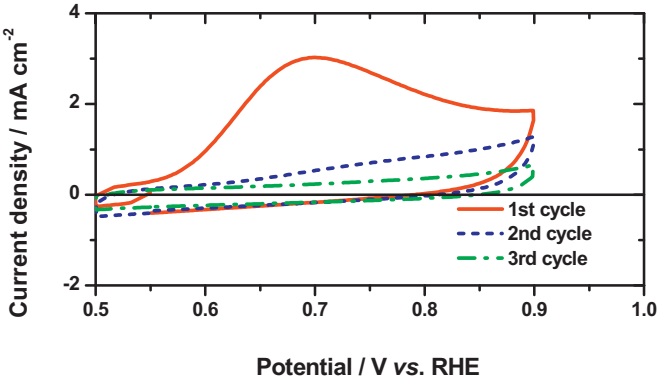

Fig. 3. Cyclic voltammograms of Pt/C in 1 M KOH–0.1 M NH_3 during the tenth-consecutive measurements at 25 °C. Sweep range: 0.50–0.90 V; scanning rate: 20 mV s^{-1}.

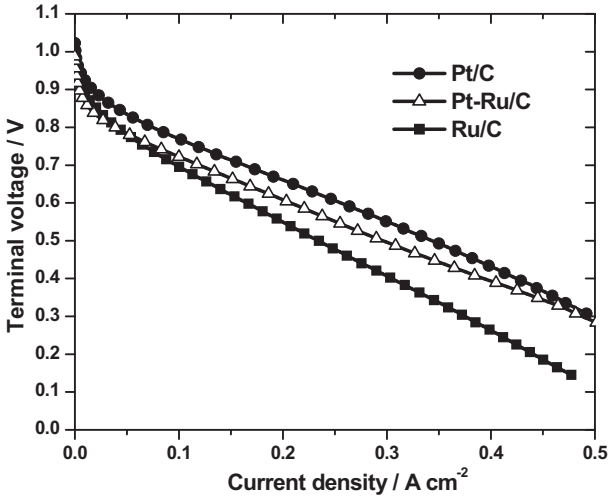

Fig. 4. *I–V* characteristics of AEM fuel cells using Pt/C (●), Ru/C (■), and Pt–Ru/C (△) as anodes. Operating temperature: 50 °C; anode gas: H_2 (humidified at 50 °C); cathode gas: O_2–N_2 (humidified at 50 °C); scanning rate: 1 mV s^{-1}.

cells [28,29]. Although the metal loading amount of Ru/C was twice larger than that of the others, the current density achieved was the lowest. This result indicates the lower activity of Ru/C for the hydrogen oxidation than that of platinum-based catalysts. Hereafter, these three cells were used for the fundamental studies on direct ammonia fuel cells.

3.3. Direct ammonia fuel cells

Fig. 5 shows the time course of OCV with a supply of hydrogen or ammonia for the three types of the fuel cells using Pt/C, Ru/C, or Pt–Ru/C anodes. The remarkable difference in OCV was observed in ammonia fuel depending on anode materials while all the cells exhibited the comparable OCV in hydrogen fuel. The obtained OCVs were 0.37 V, 0.08 V, and 0.54 V for Pt/C, Ru/C, and Pt–Ru/C, respectively. This difference in OCV reflects the catalytic activity of each catalyst for ammonia oxidation. Since the reduction in OCV will be also induced by the permeation of ammonia fuel across the AEM, the exhaust gas in the cathode side was analyzed by mass spectrometry. In this measurement, the fuel cell with Pt/C anode was exposed to H_2 and subsequently NH_3 at 20 °C. The time courses of OCV and corresponding changes in mass spectra of N_2 (m/e = 28) and NO (m/e = 30) in the exhaust gas are shown in Fig. 6. The OCV started to drop down to ca. 0.4 V within 5 min after the change in the supply gas from hydrogen to ammonia. Note that

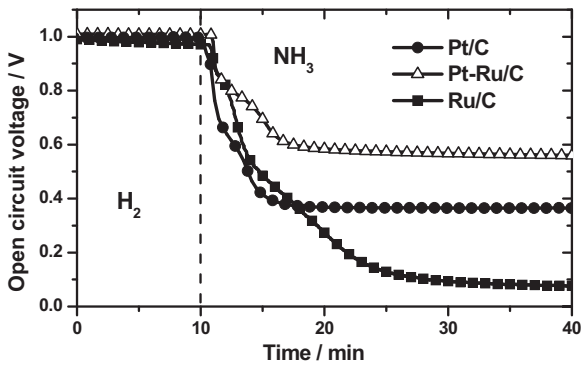

Fig. 5. Time course of open circuit voltage for AEM fuel cells using Pt/C (●), Ru/C (■), and Pt–Ru/C (△) as anodes. Operating temperature: 50 °C; anode gas: H_2 or NH_3 (humidified at 50 °C); cathode gas: O_2–N_2 (humidified at 50 °C).

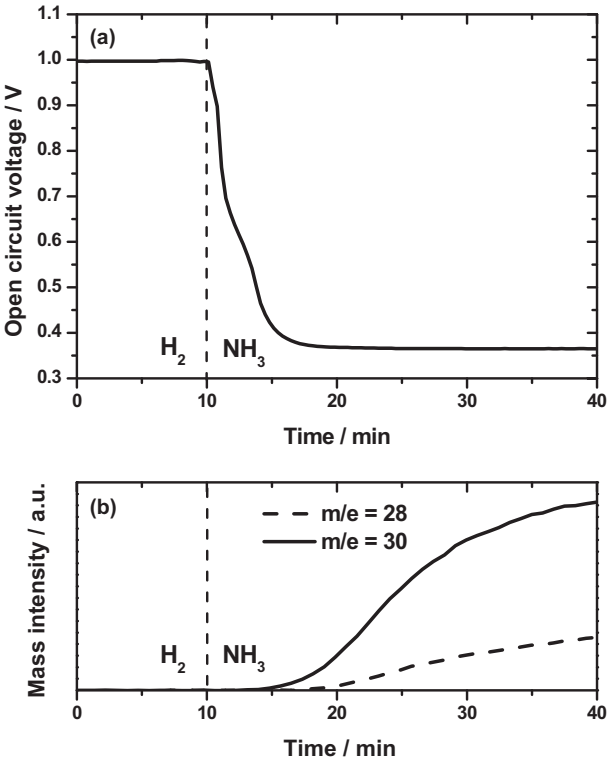

Fig. 6. Time course of (a) open circuit voltage for the AEM fuel cell with Pt/C anode and (b) mass signals in cathode exhaust gas. Operating temperature: 20 °C; anode gas: H_2 or NH_3 (humidified at 20 °C); cathode gas: O_2–Ar (humidified at 20 °C).

in response to this behavior, the mass signals of N_2 and NO were detected. Therefore, it is clarified that ammonia fuel is permeable through the AEM and then oxidized to N_2 and NO on the cathode. Next, the ammonia permeation flux across the AEM was quantitatively measured. Fig. 7 shows the variation in NH_3 flux across the AEM against the partial pressure of NH_3 in the supply gas under wet and dry conditions. The NH_3 flux changed linearly with an increase in NH_3 partial pressure under both wet and dry conditions. Thus, the noticeable amount of NH_3 was permeated under the humidified condition, which was sixty times larger than that in the dry condition. From these results, it can be concluded the NH_3 permeation across the AEM obeyed the solubility-diffusion mechanism [25]. The permeability coefficient calculated by Eq. (2) was 1.26×10^{-6} (cm^3 (STP) cm cm^{-2} s^{-1} cm Hg^{-1}) in the humidified condition, which was about two thousand times larger than

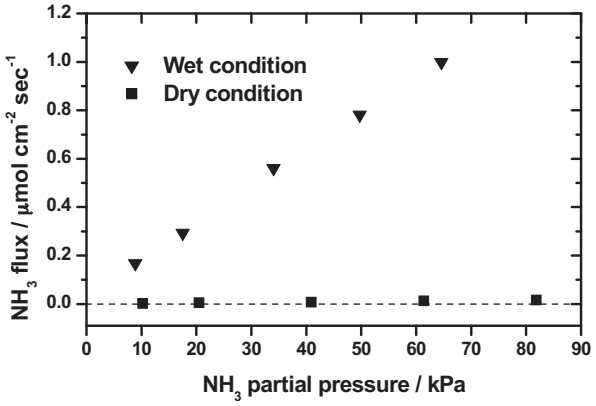

Fig. 7. NH_3 flux across the AEM at 50 °C as a function of NH_3 partial pressure in dry and wet conditions.

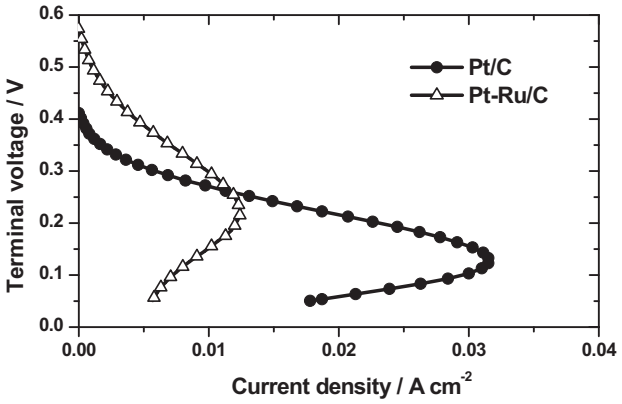

Fig. 8. *I–V* characteristics of AEM fuel cells using Pt/C (●) and Pt–Ru/C (△) as anodes. Operating temperature: 50 °C; anode gas: NH_3 (humidified at 50 °C); cathode gas: O_2–N_2 (humidified at 50 °C); scanning rate: 1 mV s^{-1}.

that of hydrogen (6.6×10^{-10} (cm^3 (STP) cm cm^{-2} s^{-1} cm Hg^{-1})). These results indicate that the considerable amount of ammonia permeated and was oxidized on the cathode under the experimental condition in Fig. 6. Thus, the permeation of NH_3 also affected the reduction in OCV in the direct ammonia fuel cell.

Fig. 8 displays the *I–V* characteristics of direct ammonia fuel cells with Pt/C and Pt–Ru/C anodes. For the cell with Ru/C, the performance test has not been conducted because of low OCV. The current densities achieved by fuel cells were about one order of magnitude smaller than those fed with hydrogen fuel. The cell with Pt/C exhibited higher current density than the cell with Pt–Ru/C, which corresponded to the result in an alkaline aqueous solution shown in Fig. 2. Note that a decrease in current density was initiated at the terminal voltages of ca. 0.15 V and ca. 0.20 V for the cells with Pt/C and Pt–Ru/C, respectively. Then, three consecutive discharge operation was conducted for the cell with Pt/C to clarify this unusual behavior and results are shown in Fig. 9. In this experiment, the cell was held at the open circuit state for 2 min between each operation. During the measurements, the current density and OCV were reduced with repeated running. However, the degraded performance was completely recovered by the discharge treatment at 0.1 A cm^{-2} for 1 min in hydrogen fuel (not shown). This indicates the degradation resulted from anode deterioration in ammonia fuel. Although N_{ad} species accumulated on Pt surface leads to the degradation of catalytic activity, they can be reductively stripped in hydrogen adsorption region as is observed in Figs. 2 and 3. Therefore, it can be concluded that the accumulation of N_{ad} over anode

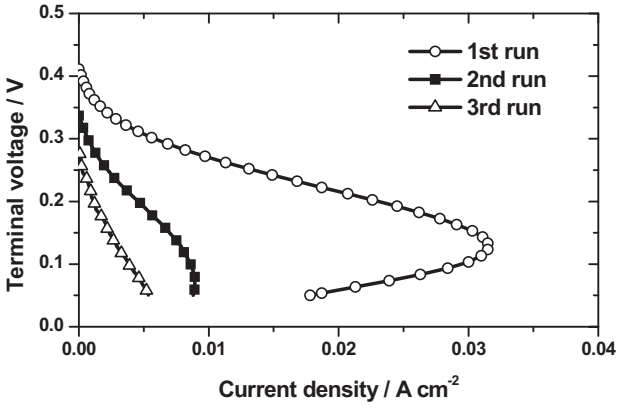

Fig. 9. *I–V* characteristics of the AEM fuel cell using Pt/C anode. Operating temperature: 50 °C; anode gas: NH_3 (humidified at 50 °C); cathode gas: O_2–N_2 (humidified at 50 °C); scanning rate: 1 mV s^{-1}.

reduced the cell performance, and the reductive desorption of N_{ad} under discharge in hydrogen fuel recovered the performance. A series of this degradation-recovery was also observed for the cell with Pt–Ru/C anode.

This study revealed that the deactivation in direct ammonia fuel cells was related to N_{ad} absorption over anode catalysts. This finding has not been reported in elsewhere to the best of our knowledge. The AEMs used in the previous studies showed extremely low performance which will be mainly due to the large ohmic loss and cathodic overpotential [16]. In such a case, it is difficult to detect the performance deterioration, since the accumulation of N_{ad} on Pt surface initiates above 0.56 V (vs. RHE). In the same reason, in AFCs with a direct ammonia supply [9–11], a large loading amount of platinum on electrodes (Pt loading amount: 51 mg cm^{-2}) would obscure the appearance of performance deterioration.

4. Conclusion

The fundamental characteristics of direct ammonia fuel cell with AEM were evaluated. The OCVs clearly depended on the electrocatalysts; the order of OCV was Pt–Ru/C > Pt/C > Ru/C. The ammonia crossover through the AEM proceeded by the solubility–diffusion mechanism, leading to the oxidation of ammonia in the cathode. Thus these two factors resulted in the reduction in OCV. Furthermore, the performance of direct ammonia fuel cells severely degraded by the accumulation of N_{ad} on the anode. This deterioration induced by N_{ad} accumulation could be recovered by the current loading treatment in hydrogen fuel. Throughout this study, it was clarified that the enhancement of electrocatalytic activity of the anodes was the important development strategy for the realization of direct ammonia fuel cells.

Acknowledgments

A part of this work was supported by Advanced Low Carbon Technology Research and Development Program (ALCA) of Japan Science and Technology Agency (JST). We thank Tokuyama Corporation for the supply of anion exchange membrane (A201) and anion exchange ionomer (AS-4), and the measurement of hydrogen permeability.

References

[1] H. Liu, C. Song, L. Zhang, H. Wang, D.P. Wilkinson, J. Power Sources 155 (2006) 95–110.
[2] B.H. Liu, Z.P. Li, J. Power Sources 187 (2009) 291–297.
[3] K. Kordesch, V. Hacker, J. Gsellmann, M. Cifrain, G. Faleschini, P. Enzinger, R. Fankhauser, M. Ortner, M. Muhr, R.R. Aronson, J. Power Sources 86 (2000) 162–165.
[4] C.H. Christensen, T. Johannessen, R.Z. Sørensen, J.K. Nrskov, Catal. Today 111 (2006) 140–144.
[5] R. Metkemeijer, P. Achard, Int. J. Power Sources 49 (1994) 271–282.
[6] F.A. Uribe, S. Gottesfeld, T.A. Zawodzinski, J. Electrochem. Soc. 149 (2002) A293–A296.
[7] R. Halseid, P.J.S. Vie, R. Tunold, J. Power Sources 154 (2006) 343–350.
[8] R. Halseid, J.S. Wainright, R.F. Savinell, R. Tunold, J. Electrochem. Soc. 154 (2007) B263–B270.
[9] E.J. Cairns, E.L. Simons, A.D. Tevebaugh, Nature 217 (1968) 780–781.
[10] E.L. Simons, E.J. Cairns, D.J. Surd, J. Electrochem. Soc. 116 (1969) 556–561.
[11] D.W. McKee, A.J. Scarpellino, I.F. Danzing, M.S. Pak, J. Electrochem. Soc. 116 (1969) 562–568.
[12] J.R. Varcoe, R.C.T. Slade, Fuel Cells 5 (2005) 187–200.
[13] G.F. Mclean, T. Niet, S. Prince-Richard, N. Dijilali, Int. J. Hydrogen Energy 27 (2002) 507–526.
[14] A. Tewari, V. Sambhy, M.U. Macdonald, A. Sen, J. Power Sources 153 (2006) 1–10.
[15] L.A. Adams, S.D. Poynton, C. Tamain, R.C.T. Slade, J.R. Varcoe, ChemSusChem 1 (2008) 79–81.
[16] R. Lan, S. Tao, Electrochem. Solid-State Lett. 13 (2010) B83–B86.
[17] H. Gerischer, A. Mauerer, J. Electroanal. Chem. 25 (1970) 421–433.
[18] J.F.E. Gootzen, A.H. Wonders, W. Visscher, R.A. van Santen, J.A.R. van Veen, Electrochim. Acta 43 (1998) 1851–1861.

[19] F.J. Vidal-Iglesias, J. Solla-Gullón, J.M. Feliu, H. Baltruschat, A. Aldaz, J. Electroanal. Chem. 588 (2006) 331–338.
[20] A.C.A. de Vooys, M.T.M. Koper, R.A. van Santen, J.A.R. van Veen, J. Electrochem. Soc. 506 (2001) 127–137.
[21] A.C.A. de Vooys, M.F. Mrozek, M.T.M. Koper, R.A. van Santen, J.A.R. van Veen, M.J. Weaver, Electrochem. Commun. 3 (2001) 293–298.
[22] F.J. Vidal-Iglesians, J. Solla-Gullon, A. Perez, A. Aldaz, Electrochem. Commun. 8 (2006) 102–106.
[23] K. Endo, K. Nakamura, Y. Katayama, T. Miura, Electrochim. Acta 49 (2004) 2503–2509.
[24] F.J. Vidal-Iglesias, J. Solla-Gullón, V. Montiel, J.M. Feliu, A. Aldaz, J. Power Sources 171 (2007) 448–456.
[25] Y. He, E.L. Cussler, J. Membr. Sci. 68 (1992) 43–52.
[26] F. Vitse, M. Cooper, G.G. Botte, J. Power Sources 142 (2005) 18–26.
[27] J.R. Varcoe, R.C.T. Slade, Electrochem. Commun. 8 (2006) 839–843.
[28] C. Tamain, S.D. Poynton, R.C.T. Slade, B. Carroll, J.R. Varcoe, J. Phys. Chem. C 111 (2007) 18423–18430.
[29] S.D. Poynton, J.P. Kizewski, R.C.T. Slade, J.R. Varcoe, Solid State Ionics 181 (2010) 219–221.